frontiers | Frontiers in Oncology

TYPE Original Research
PUBLISHED 29 November 2022
DOI 10.3389/fonc.2022.1021823

OPEN ACCESS

EDITED BY
Bekir Cinar,
Clark Atlanta University, United States

REVIEWED BY
Andrew Newby,
University of Bristol, United Kingdom
Xianjue Ma,
Westlake University, China

*CORRESPONDENCE
Jyoti R. Misra
jyoti.misra@utdallas.edu

SPECIALTY SECTION
This article was submitted to Cancer Molecular Targets and Therapeutics, a section of the journal Frontiers in Oncology

RECEIVED 17 August 2022
ACCEPTED 02 November 2022
PUBLISHED 29 November 2022

CITATION
Gridnev A, Maity S and Misra JR (2022) Structure-based discovery of a novel small-molecule inhibitor of TEAD palmitoylation with anticancer activity. *Front. Oncol.* 12:1021823. doi: 10.3389/fonc.2022.1021823

Structure-based discovery of a novel small-molecule inhibitor of TEAD palmitoylation with anticancer activity

Artem Gridnev, Subhajit Maity and Jyoti R. Misra*

Department of Biological Sciences, University of Texas at Dallas, Richardson, TX, United States

The paralogous oncogenic transcriptional coactivators YAP and TAZ are the distal effectors of the Hippo signaling pathway, which plays a critical role in cell proliferation, survival and cell fate specification. They are frequently deregulated in most human cancers, where they contribute to multiple aspects of tumorigenesis including growth, metabolism, metastasis and chemo/immunotherapy resistance. Thus, they provide a critical point for therapeutic intervention. However, due to their intrinsically disordered structure, they are challenging to target directly. Since YAP/TAZ exerts oncogenic activity by associating with the TEAD1-4 transcription factors, to regulate target gene expression, YAP activity can be controlled indirectly by regulating TEAD1-4. Interestingly, TEADs undergo autopalmitoylation, which is essential for their stability and function, and small-molecule inhibitors that prevent this posttranslational modification can render them unstable. In this article we report discovery of a novel small molecule inhibitor of YAP activity. We combined structure-based virtual ligand screening with biochemical and cell biological studies and identified JM7, which inhibits YAP transcriptional reporter activity with an IC50 of 972 nMoles/Ltr. Further, it inhibits YAP target gene expression, without affecting YAP/TEAD localization. Mechanistically, JM7 inhibits TEAD palmitoylation and renders them unstable. Cellular thermal shift assay revealed that JM7 directly binds to TEAD1-4 in cells. Consistent with the inhibitory effect of JM7 on YAP activity, it significantly impairs proliferation, colony-formation and migration of mesothelioma (NCI-H226), breast (MDA-MB-231) and ovarian (OVCAR-8) cancer cells that exhibit increased YAP activity. Collectively, these results establish JM7 as a novel lead compound for development of more potent inhibitors of TEAD palmitoylation for treating cancer.

KEYWORDS

YAP, TEAD, hippo signaling, cancer, small-molecule inhibitor; virtual ligand screening

Introduction

The Hippo signaling pathway is a conserved signaling network that plays a critical role in cell proliferation, survival, differentiation and tissue homeostasis (1, 2). The pathway consists of a core kinase cascade that negatively regulates the paralogous oncogenic transcriptional coactivators, Yes Associated Protein (YAP) and Transcriptional Activator with PDZ-binding motif (TAZ). The kinase cascade consists of the serine threonine kinases MST1/2 and Large Tumor Suppressor 1/2 (LATS1/2), and their obligate adapters SAV and MOB1A/B respectively, where MST1/2 phosphorylates and activates LATS1/2, which in turn phosphorylates YAP/TAZ. Lats1/2 can also be phosphorylated and activated by MAP4K1-7 and Tao1/3 kinases (3, 4). Phosphorylated YAP/TAZ gets sequestered in the cytoplasm and gets ubiquitinated and degraded. Under low Hippo pathway activity, hypo/unphosphorylated YAP/TAZ translocates into the nucleus, where it associates with various transcription factors such as TEAD1-4, SMAD3 and RUNX (5, 6). Of these transcription factors, TEAD1-4 mediate the regulation of majority of the YAP-target genes, which encode various cytokines and matricellular proteins that promote cell proliferation and inhibit apoptosis.

YAP/TAZ has emerged as a central player in many cancers including breast, colorectal, liver, lung, pancreas, thyroid and sarcomas (7, 8). Despite these observations, point mutations within the Hippo pathway components are relatively rare in most cancers. Most cancers harbor mutations in the upstream regulators that promote elevated expression and nuclear localization of YAP/TAZ. One of the key upstream regulators of YAP is Merlin, which is encoded by the NF2 gene. Merlin plays an important role in recruiting the core components of the Hippo signaling pathway to the plasma membrane, facilitating activation of the LATS1/2 kinase (9). Germline loss-of-function mutations or deletion of NF2 results in neurofibromatosis type 2, which causes bilateral vestibular schwannomas (10). Somatic mutations of NF2 are also observed in spontaneous schwannomas, meningiomas, mesothelioma and renal cell cancer. A comprehensive study of 32 different cancers revealed that malignant mesothelioma has the highest frequency of NF2 mutations (11, 12). Similarly, a large proportion of meningiomas harbor mutations in NF2 (13). Furthermore, 6% of non-small-cell lung cancer exhibit YAP amplification, while 29% of them show TAZ amplification (14). YAP is also frequently amplified in head and neck cancers. 90% of epithelioid hemangioendothelioma (EHE), a rare vascular sarcoma, harbor TAZ-CMTA1 fusion while 10% of EHE have YAP-TFE3 fusion (15–18). In addition to these, oncogenic mutations that activate growth promoting signaling pathways such as EGFR, RAS-MAPK, PI3K and Wnt signaling also promote higher YAP/TAZ expression.

Overexpressed YAP/TAZ undergoes phase separation at the super enhancers and promotes sustained expression of the target genes (19–21). Genetic analyses revealed that YAP contributes to multiple aspects of cancer development, including growth, survival, metabolism and metastasis. It also plays an important role in cancer fibroblast proliferation and ECM deposition. They also promote cancer stem cell fate maintenance and chemotherapy resistance (22, 23). Furthermore, YAP promotes expression of the chemokine CXCL5, which results in the recruitment of myeloid cells that suppress T-cells (24). In regulatory T-cells (Tregs) YAP supports FOXP3 expression *via* activin signaling and Treg function. Accordingly, YAP deficiency results in dysfunctional regulatory T cells (Tregs), which are no longer able to suppress antitumor immunity (25). YAP upregulates PD-L1 expression in the cancer cells, and by this mechanism directly mediates evasion of cytotoxic T-cell immune responses (19, 22, 26–28). Thus, YAP/TAZ regulates multiple aspects of tumorigenesis, and provides a critical control point for therapeutic intervention for cancer treatment. However, it is challenging to directly inhibit YAP/TAZ, since it is an intrinsically disordered protein. Similarly, it is difficult to interfere YAP-TEAD1-4 interaction with small-molecules, as the interaction interface is very broad, shallow, and exposed to solvent, although a few molecules that bind to the interface-2 have been reported to achieve this. Several groups have developed linear and cyclic peptides and small molecules that bind to TEAD and interfere with YAP/TAZ-TEAD interaction (29–31). However, these molecules exhibit poor efficacy or cell permeability, which has limited their use. Therefore, recent efforts are aimed at alternate approaches to inhibit YAP activity indirectly, by disrupting TEAD function.

TEAD transcription factors undergo covalent modification with palmitic acid at a conserved cysteine residue and are depalmitoylated by the APT2 and ABHD17 depalmitoylases (32, 33). The palmitic acid occupies a central hydrophobic pocket in these proteins and regulates their stability and activity. Inhibition of TEAD palmitoylation can render these proteins unstable, and allosterically interferes with their interaction with YAP/TAZ (34–36). Further, a small molecule inhibitor that binds to the palmitic acid binding pocket is known to exert a dominant negative effect on TEAD binding to the chromatin and converts TEAD from a transcriptional activator to a transcriptional repressor (35). Interestingly, the central hydrophobic pocket is highly druggable, and more importantly, structural alignment has revealed that 75% of the residues are identical and the other 25% of the residues are 75% similar across all the 4 TEAD isoforms (8). Thus, it is possible to develop pan-TEAD inhibitors that bind to this region. Several investigational compounds have been reported to bind to this site and inhibit YAP activity (29, 30). However, due to high failure rates during clinical trials and potential development of resistance, there is a continuing urgent need for developing novel chemotype-based potent TEAD inhibitors.

Recent developments in structure-based virtual ligand screening (VLS) allows one to conduct *in silico* screening of large libraries of small molecules to predict the ones, which have

high probability of binding to a given site in a target protein (37–39). This significantly reduces the time, labor and cost to identify potential hit compounds. Here we report isolation of a novel small molecule that inhibits YAP transcriptional activity. Using structure based VLS combined with cell biological and biochemical analyses we identified JM7 as a potent inhibitor of TEAD palmitoylation. It negatively regulates TEAD stability and YAP target gene expression. Furthermore, we show that this compound inhibits, proliferation, colony formation and migration of breast and ovarian cancer cell lines that exhibit high YAP/TAZ activity.

Results

Molecular docking-based identification of JM7

To identify potential small-molecule inhibitors that bind to the TEAD central pocket, where the palmitic acid normally resides, we conducted a structure-based VLS. To achieve this, we used the crystal structure of TEAD2 with PDB ID 6UYC and prepared it for docking using the Protein Preparation Wizard in Glide. This structure has a resolution of 1.66 angstroms and is co-crystalized with a ligand that binds with 229 nanomolar affinity (35). We generated a library of about 600,000 small molecules from PubChem and prepared the ligands for docking using Ligprep Wizard in Glide. After performing standard precision (SP) docking the top 2% compounds were subjected to extra precision (XP) docking in Glide. Finally, Molecular Mechanics with Generalized Born and Surface Area Solvation (MM/GBSA) was performed to allow 5 angstroms movement of the protein structure. The top 50 compounds with highest free energy of binding (dG-bind score) were purchased and examined if they inhibit YAP transcriptional activity.

To screen the compounds for inhibiting YAP-transcriptional activity, we generated a stable HEK-293 cell line that enables to monitor YAP-TAZ/TEAD transcriptional activity, by infecting with a lentivirus carrying 8 tandem copies of the TEAD binding site from the SV40 enhancer (8XGTIIC), upstream of a Firefly luciferase (Fluc). To normalize this reporter activity, we either measured the ATP levels by CellTiterGlow™ or transfected with a plasmid expressing Renilla luciferase from the HSV thymidine kinase promoter (Rluc). Given that the basal Fluc activity of the 8XGTIIC-Fluc reporter is low, we transfected these cells with plasmids encoding unphosphorylatable YAP (YAP5SA) or TAZ (TAZS89A) mutants. Expression of these mutant proteins dramatically activated the Fluc expression, as expected, without affecting Rluc expression (Figures S1A, B). We then treated these cells with 10uM of the compounds to examine if they inhibited the reporter activation. From this screen we identified a compound JM7 (Figure 1A), which inhibited the YAP transcriptional reporter, without causing any apparent effect on cell viability. Further, since many small molecules can inhibit Fluc activity nonspecifically, we also examined if JM7 inhibits Fluc activity. To do this we transfected HEK-293 cells with a plasmid expressing Fluc from the SV40 promoter and treated with DMSO alone or 2 micromolar JM7 and measured Fluc activity and found that JM7 does not inhibit Fluc activity (Figure S1C). Thus, JM7 specifically inhibits the 8XGTIIC reporter. It is predicted to bind to the TEAD central pocket mostly through hydrophobic interactions, hydrogen bonding with Ser345, and pi-pi stacking with Tyr426 (Figures 1B–D).

To examine if JM7 inhibits YAP/TAZ activity in a dose-dependent manner, we treated HEK293-8XGTIIC cells expressing YAP 5SA or TAZ S89A with DMSO alone, or 1, 2 or 5 micromolar JM7 overnight and examined how they affected YAP transcriptional activity. We observed that JM7 caused a dose-dependent decrease in Fluc expression induced by YAP 5SA (Figures 2A, A") and TAZ S89A (Figure 2B-B"). In parallel we performed CellTiter Glow™ assay, which measures the general cell viability. We observed no significant decrease in CellTiter Glow activity in cells treated with different doses of JM7 compared to the vehicle treated controls cells (Figures 2A', B'). To determine the IC50 value of JM7, we transfected HEK293 cells expressing the 8XGTIIC-Fluc reporter with plasmids encoding Rluc and YAP5SA, following which we treated them with logarithmic concentrations of JM7 and determined the concentration at which it inhibits Fluc activity by 50% (Figure 2C). In parallel, we also measured the Rluc expression (Figure 2D). We observed that JM7 caused a 50% inhibition of Fluc expression at 972 nanomolar concentration. Together, these experiments indicate that JM7 inhibits YAP transcriptional activity in a dose-dependent manner with an IC50 value of 972 nanomolar.

JM7 inhibits YAP target gene expression

Encouraged by the effect of JM7 on YAP/TAZ transcriptional reporter activity, we then sought if it affects the expression of YAP/TAZ target genes. *CTGF* and *CYR61* are two of the well characterized YAP target genes and are overexpressed in cancer cells that exhibit increased YAP activity. MDA-MB-231 is a triple negative breast cancer cell line that harbors a deletion in the NF2 gene, and therefore, exhibits increased YAP activity. Similarly, OVCAR-8 ovarian cells overexpress TEAD4. Therefore, we treated MDA-MB-231 and OVCAR-8 cells with DMSO alone or 1 or 2 micromolar JM7 and examined the CTGF and CYR61 transcript levels by quantitative reverse transcription polymerase chain reaction (qRT-PCR). GAPDH transcript levels were used for normalizing the expression levels. We observed that JM7 significantly downregulated the expression of both CTGF and CYR61 transcript levels in a dose dependent manner, in both MDA-MB- 231 and OVCAR-8 cells (Figures 3A, B).

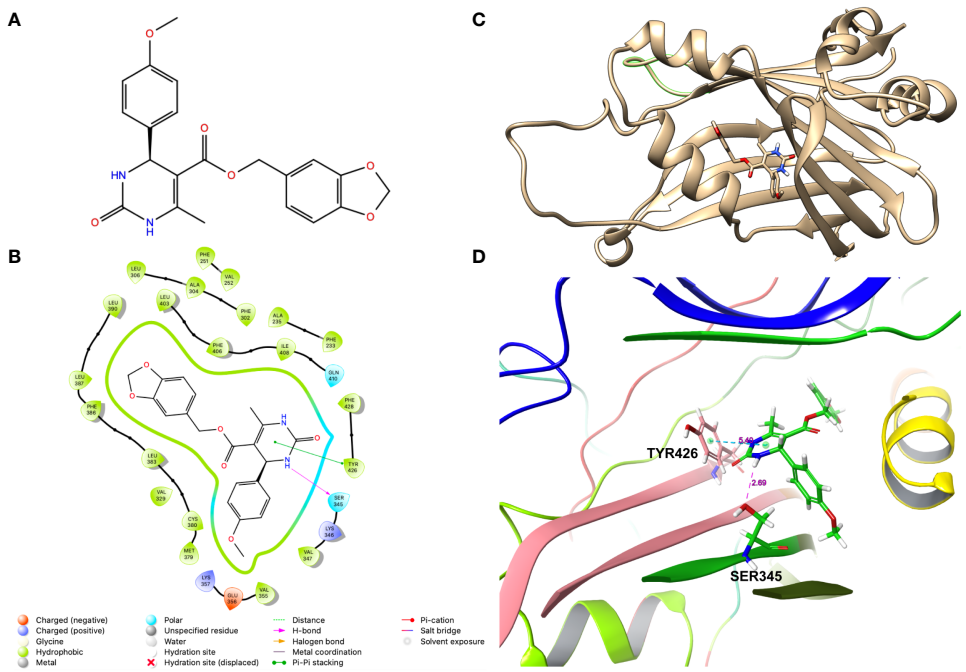

FIGURE 1
JM7 is predicted to bind to the TEAD cetral pocket. **(A)** Chemical structure of JM7. **(B)** Structure of TEAD2 (PDB ID: 6UYC) with predicted binding pose of JM7 and enlarged view **(D)**. **(C)** Schematic showing the ligand interaction diagram for JM7. Dotted lined indicate the pi-pi stacking between JM7 and TYR426 and hydrogen bond between JM7 and Ser345. Numbers indicate distances in Angstroms.

Similar dose dependent effect on decrease of CTGF and CYR61 transcript levels were also observed in NF2 mutant NCI-226 mesothelioma cells (Figures S3A, B). Together, these results indicate that JM7 not only inhibits YAP transcriptional reporter activity, but also inhibits YAP target gene expression.

JM7 does not affect nuclear localization of YAP and TEAD

YAP and TEAD activity is primarily controlled by their nuclear localization, and an inhibitor can block their activity, potentially, by affecting their levels and preventing their nuclear translocation. Therefore, we examined if JM7 affects YAP/TEAD localization in MDA-MB-231 and OVCAR-8 cells. We treated these cells with DMSO alone or 2uM or 5uM JM7 and stained with α-YAP and α-TEAD antibodies and counterstained the nuclei with Hoechst. In the DMSO treated cells, as expected, TEAD primarily localized to the nucleus and YAP localized to both cytoplasm and the nucleus. Similarly, JM7 treated cells displayed similar localization of YAP and TEAD as the DMSO treated cells (Figure 3C–J", Figure S2). Further, JM7 did not affect subcellular localization of YAP and TEAD in NCI-H226 cells as well (Figure S4). These results suggest that JM7 does not affect YAP/TEAD nuclear localization to inhibit their transcriptional activity.

JM7 inhibits protein stability and palmitoylation of TEAD

Palmitoylation is critical for TEAD stability, and inhibition of this modification with certain small-molecule inhibitors that bind to the central pocket can destabilize these proteins. However, one small-molecule TEAD inhibitor that binds to the palmitic acid binding pocket was reported to stabilize TEAD, but dominant negatively interfere with its association with chromatin (35). In order to examine how JM7 affects TEAD stability, we transfected HEK293 cells with plasmids encoding Myc-TEAD1-4 and treated them with either DMSO or 2uM JM7 for 24 hours and examined the levels of Myc-TEAD by Western blotting, using anti-Myc antibody. We observed that JM7 affects the stability of all four TEAD isoforms (Figures 4A–D input lanes). Further, to examine if JM7 induces proteosomal degradation of TEAD1-4, we transfected HEK-293 cells with plasmids expressing Flag: TEAD1, Myc : TEAD2, V5:TEAD3 and HA : TEAD4 and treated with either DMSO, 2uM JM7 witout or with 500nM of the proteosomal inhibitor MG132. Subsequently, the effect on TEAD1-4 levels was analysed by Western blotting using antibodies against the epitope tags. As expected, JM7 treatment induced degradation of all 4 TEAD isofroms. Interestingly, MG132 treatment reversed the

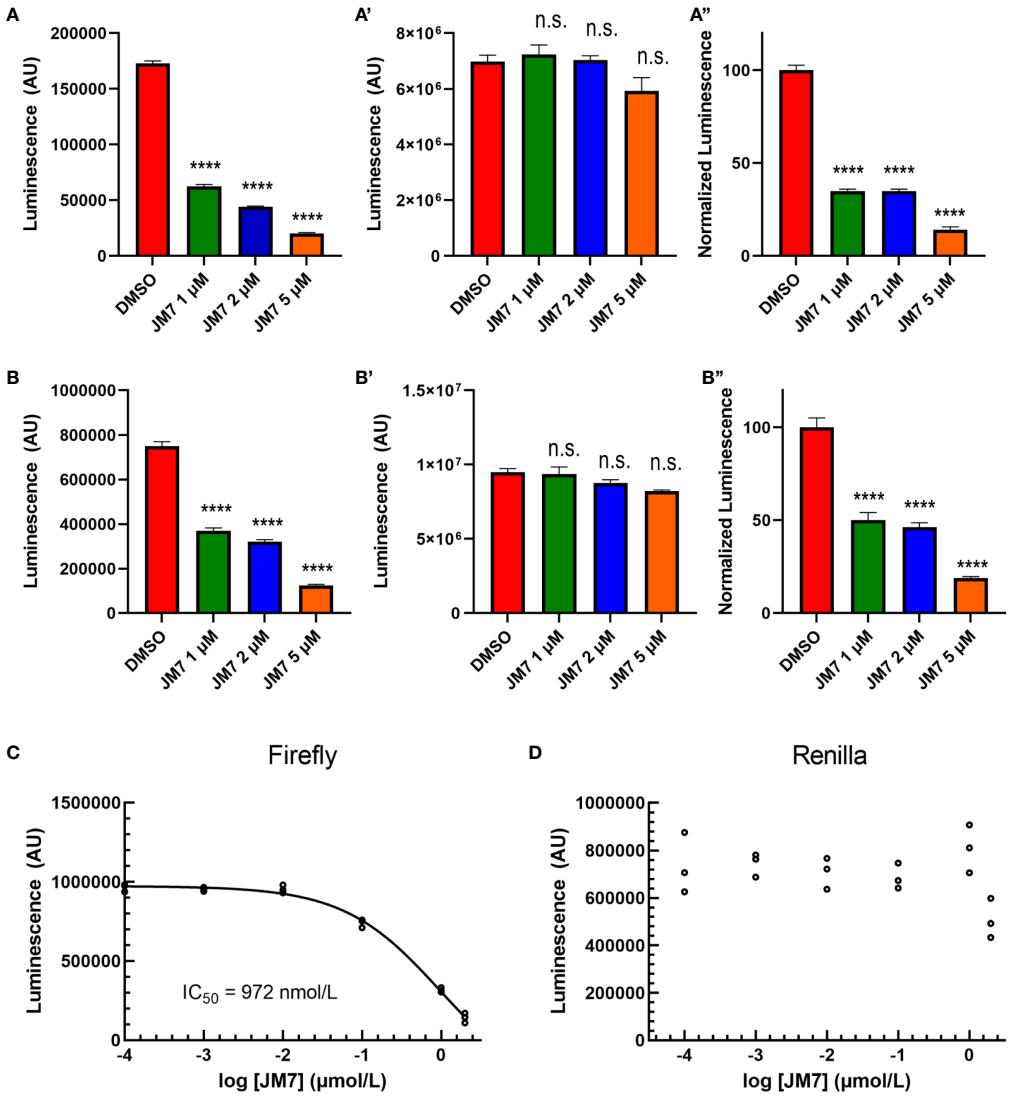

FIGURE 2
JM7 inhibits YAP/TAZ transcriptional activity. **(A, B")** Luciferase reporter activity **(A, B)**, Cell Titer Glow activity **(A', B")** and the normalized luciferase reporter activity (ratio of Luciferase reporter activity to Cell Titer Glow activity normalized to DMSO treated cells) **(A", B")** in HEK293 cells carrying 8xGTIIC-Luc and expressing YAP5SA **(A-A")** or TAZ S89A **(B-B")**, treated with DMSO or indicated doses of JM7 showing dose dependent inhibition of reporter activity without apparent effect on cell titer glow activity. **(C, D)** Normalized Firefly luciferase or Renilla luciferase activity in HEK293 cells carrying 8xGTIIC-FLuc, pCMV-RLuc and YAP5SA treated with different doses of JM7 showing IC50 value of 972nM. ****=p<0.0001, ns, not significant. Error bars indicate Standard Error of Mean (SEM) of 3 replicates.

destabilizing effect of JM7 on TEAD1-4, suggesting that JM7 induces proteosomal degradation of TEAD1-4 (Figure S3).

Since JM7 was predicted to bind to the central hydrophobic pocket that is normally occupied by the palmitic acid, we sought to examine if it affects TEAD palmitoylation. To address this, we transfected HEK-293 cells with plasmids expressing Myc epitope tagged TEAD1-4 and treated them with alkyne palmitic acid along with DMSO or 2 micromolar JM7 for 24 hours. Myc-TEAD1-4 was subsequently immunoprecipitated using anti-Myc affinity resins and the alkyne palmitate was covalently conjugated with azide-biotin using click chemistry. Subsequently, palmitoylated TEAD1-4 was detected by Western blotting with fluorescently labeled streptavidin, and the total amount of TEAD was detected with anti-Myc antibody. Because JM7 treatment destabilizes TEAD1-4, lesser amount of the immunoprecipitated TEAD from DMSO treated cell lysate was loaded to equalize total Myc-TEAD1-4 amounts. We observed that JM7 treatment modestly inhibited TEAD1 palmitoylation, but significantly inhibited palmitoylation of TEAD2-4, (Figures 4B–D').Together, these experiments

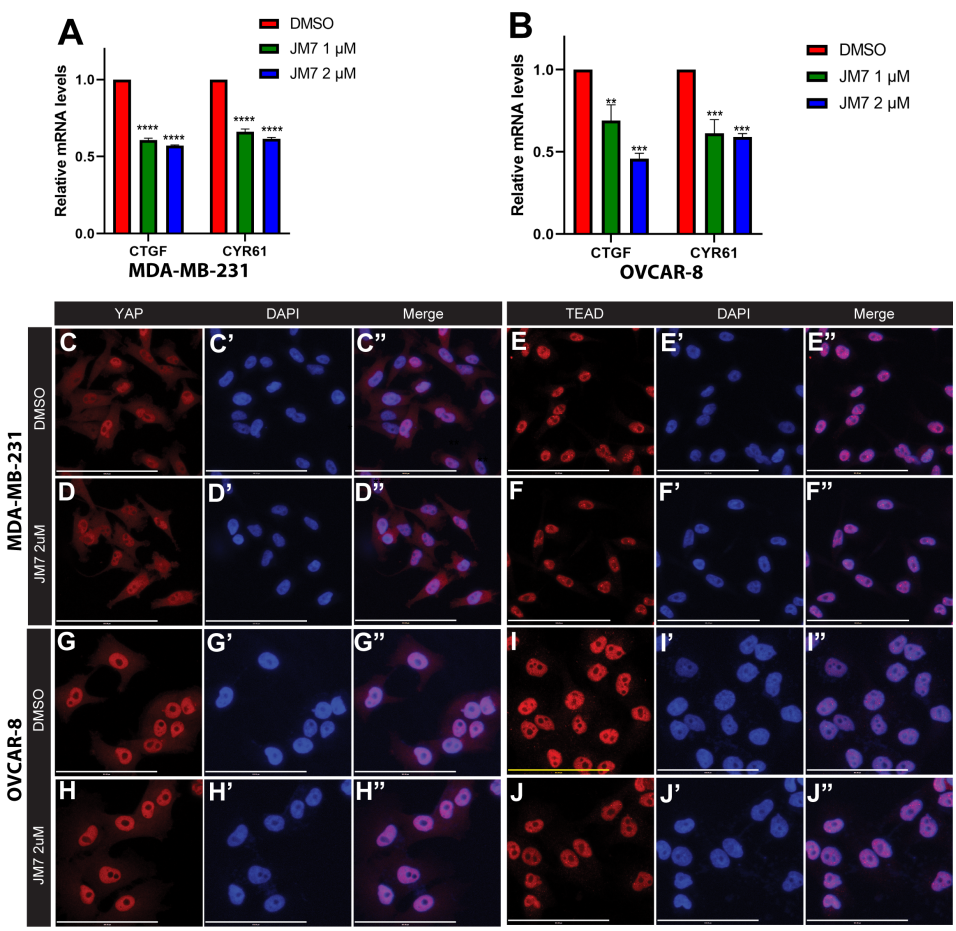

FIGURE 3
JM7 inhibits YAP target genes in breast and ovarian cancer cells and does not affect YAP or TEAD localization.**(A, B)** Histograms showing relative expression of CTGF and CYR61 mRNA levels in MDA-MB-231 **(A)** and OVCAR-8 **(B)** cells treated with DMSO or indicated doses of JM7, showing a dose dependent inhibition of these YAP target genes. **(C–J″)** MDA-MB-231 **(C–F″)** and OVCAR-8 **(G–J″)** cells were treated with DMSO or 2 micromolar JM7 and stained with TEAD or YAP antibody and Hoechst to stain the nuclei showing that JM7 does not seem to affect YAP or TEAD nuclear localization. **p<0.005; ***p<0.01; ****p<0.0005. Scale bar=100um. Error bars indicate Standard Error of Mean (SEM) of 3 replicates.

indicate that JM7 impairs TEAD stability and inhibits TEAD palmitoylation.

Consistent with the destabilizing effect on TEAD, JM7 caused inhibition of NanoBit complementation (40). In this assay, an engineered small bright Luciferase called Nanoluc is split into two fragments, a small fragment,SmBit and a large fragment, LgBit. SmBit and LgBit normally do not interact with each other to reconstitute the Nanoluc enzymatic activity. However, when these fragments are fused to two proteins such as YAP and TEAD that interact with such other, YAP-TEAD interaction brings these fragments in close proximity and reconstitutes the Nanoluc activity. Any compound that inhibits YAP-TEAD interaction would therefore cause a decrease in Nanoluc activity. This system was previously developed for YAP and TEAD-1. Now we have generated the fusion proteins to test interaction of both YAP and TAZ with all four TEAD isoforms. As expected, cells transfected with plasmids expressing just SmBit-YAP, SmBit-TAZ or LgBit-TEAD1-4 alone had very low basal NanoLuc activity (Figures S2A–D). However, cells expressing either SmBit-YAP or SmBit-TAZ together with the different isoforms of LgBit-TEAD exhibit very high NanoLuc activity (Figures S4A–D). When the cells expressing SmBit-YAP or SmBit-TAZ together with the different isoforms of LgBit-TEAD were treated with either DMSO or 2 micromolar JM7, we observed that JM7 treatment destabilized LgBit-TEAD1-4 and consistently decreased the Nanoluc activity (Figures S5A–L).

JM7 directly engages with TEAD1-4 in cells

Given that JM7 inhibits TEAD transcriptional activity and inhibits their palmitoylation, we wanted to examine if JM7 directly

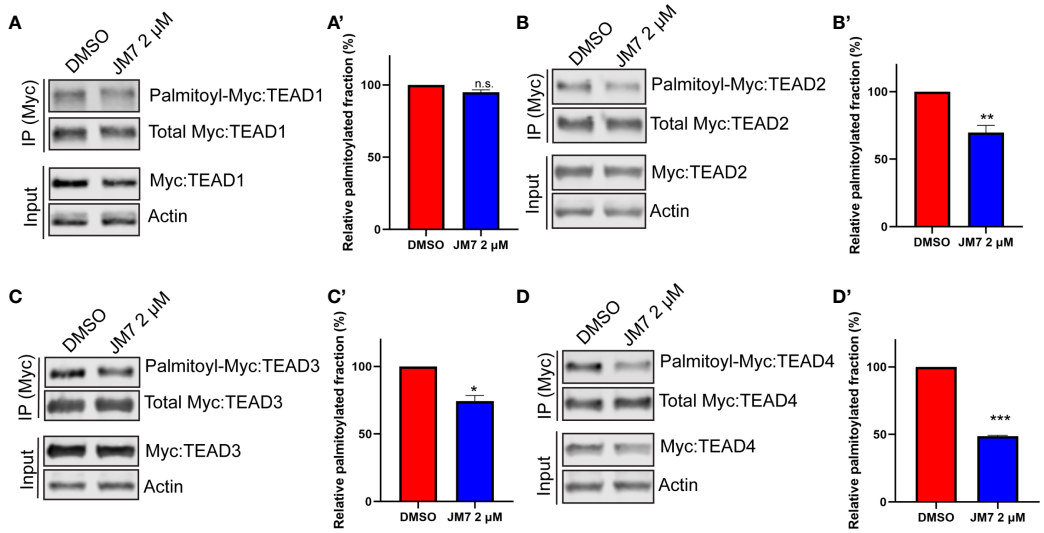

FIGURE 4
JM7 inhibits TEAD palmitoylation, impairs TEAD stability. Western blots and their quantitation showing decreased palmitoylation (in the IP lanes) and degradation (in the input lanes) of TEAD1 **(A, A')** TEAD2 **(B, B')** TEAD3 **(C, C')** and TEAD4 **(D, D')** in lysates of HEK293 cells expressing Myc tagged TEAD1-4 and treated with DMSO or 2 micromolar JM7. Actin is used as a control for equal loading and transfer of the input samples. HEK293 expressing Myc tagged TEAD1-4 were treated with DMSO or 2 micromolar JM7 along with alkyne palmitic acid. The Myc-TEAD was immunoprecipitated and the alkyne palmitic acid was covalently conjugated with azide-biotin by click chemistry and the biotin was detected by blotting with fluorescently conjugated streptavidin. Error bars indicate Standard Error of Mean (SEM) of 3 replicates. n.s: non-significant, *p< 0.05; **p<0.005; ***p<0.001.

binds to the TEADs. To test this, we performed cellular thermal shift assay (CETSA), which is based on the principle that ligand bound proteins are resistant to thermal denaturation compared to their unbound counterparts (41). We expressed Myc-tagged TEAD1-4 in HEK293 cells and treated them with either DMSO or JM7, after which we subjected the cells to thermal denaturation at a gradient of increasing temperatures. The cells were subsequently lysed by freeze thawing and the denatured proteins were separated from the non-denatured proteins by centrifugation. The supernatant containing non-denatured proteins was examined for Myc-TEAD by Western blotting using anti-Myc antibody. We observed that while at high temperature, both DMSO and JM7 treated Myc-TEAD1-4 gets denatured, at lower temperatures, JM7 treated samples contain higher amount of non-denatured Myc-TEAD, compared to DMSO treated samples, indicating that JM7 directly binds to TEAD1-4 and renders them resistant to thermal denaturation (Figures 5A–D). Together, these experiments suggest that JM7 directly engages TEAD1-4 in cells.

JM7 inhibits proliferation, colony formation and migration in MDA-MB-231, OVCAR-8 and NCI-226 cells

Since JM7 binds to TEAD and inhibits its palmitoylation, stability and YAP target gene expression, we wanted to examine if JM7 inhibits cell proliferation, colony formation and migration of MDA-MB-231, OVCAR-8 and NCI-226 cells cancer cells that exhibit high YAP activity. To test the effect of JM7 on cell proliferation, we treated MDA-MB-231 and OVCAR-8 cells with either DMSO or 2 micromolar JM7 and performed the MTT assay. In this assay, the colorless MTT reagent is converted by the cellular oxidoreductases to colored formazan crystals, which are then solubilized and quantitated by measuring the absorbance of the colored product. Thus, it provides an indirect measure of the number of cells. We observed that JM7 treatment significantly impacts the proliferation of these cancer cells (Figures 6A, B). We then examined if JM7 affects the colony forming ability of these cells. To address this, we plated equal number of MDA-MB-231 and OVCAR8 cells and treated them with DMSO or 1, 2 or 5 micromolar JM7 for 2 weeks, after which the cells were fixed and stained with crystal violet. We observed that even at 1uM dose JM7 impacted colony forming ability of the MDA-MB-231 cells. Interestingly, at 2 and 5 micromolar there was a dramatic reduction in the colony forming ability of these cells (Figures 6C, E). On the other hand, JM7 had a significant effect on the colony formation ability of OVCAR-8 at 5 micromolar (Figures 6D, F). Similarly, JM7 severely attenuated colony forming ability of NCI-H226 cells (Figures S3C, D). Finally, we wanted to examine how JM7 affects the migration of the MDA-MB-231 and OVCAR8 cells. To address this, we grew the MDA-MB-231

and OVCAR8 cells in confluent monolayers and scratched with a pipette tip. After carefully washing away the detached cells, we treated them with DMSO alone or 2 micromolar JM7 and imaged 0, 19 and 24 hours after drug treatment. We observed that while cells treated with DMSO alone gradually migrated and filled the gap over time, JM7 treatment significantly attenuated this response (Figures 6G–L). Furthermore, similar effects were observed for wound healing assays in NCI-H226 cells (Figures S3E, F).Together, these experiments indicate that JM7 inhibits proliferation, colony forming ability and migration of the MDA-MB-23, OVCAR-8 and NCI-226 cells.

Discussion

The transcriptional coactivators YAP/TAZ are the distal effectors of the Hippo signaling pathway and play a critical role in regulating cell proliferation, apoptosis and fate specification (1, 2). They regulate expression of majority their target genes by interacting with TEAD1-4 transcription factors and are frequently deregulated in several cancers, where they regulate multiple aspects of cancer development including cancer growth, metastasis and chemo/immunotherapy resistance (8). Thus, they provide a critical target for therapeutic intervention. However, it is not possible to directly target YAP/TAZ, since they are intrinsically disordered. Therefore, YAP activity can be alternatively controlled by targeting TEAD1-4, which contain a highly druggable central hydrophobic pocket that is normally occupied by a palmitic acid. Small-molecule inhibitors of TEAD palmitoylation destabilize these transcription factors by promoting their ubiquitination and thereby inhibit YAP transcriptional activity. Although a number of such experimental inhibitors exists, none has successfully completed clinical trials yet. Therefore it is important to develop inhibitors based on novel chemotypes. In this study, we undertook a structure-based computational screening of a large library of small-molecule inhibitors and identified JM7, a new-chemotype based small molecule inhibitor for TEAD palmitoylation that inhibits YAP transcriptional activity. JM7 is not similar in structure to known TEAD palmitoylation inhibitors and is thus based on novel chemical matter. It is predicted to possess many desirable physicochemical and pharmacological properties such as lipophilicity and bioavailability. It also does not violate Lipinski's rule of 5 and synthetically accessible (Supplementary Table 1). It directly binds to TEAD in cells and decreases their stability. It significantly inhibits the palmitoylation of TEAD2-4. However, JM7 only modestly inhibits TEAD1 palmitoylation, yet induces strong TEAD1 destabilization, which can be reversed by MG132 treatment. This could be due to rapid degradation of JM7 bound TEAD1, so that the immunoprecipitated TEAD1 is primarily the fraction that is not bound to JM7 and does not show a statistically significant decrease in palmitoylation. Nevertheless, JM7 induces destabilization of all 4 TEAD isofroms. Further, it inhibits proliferation, colony formation and migration of MDA-MB-231, OVCAAR-8 and NCI-226 cancer cells.

The palmitic acid binding pocket in TEAD is highly druggable. However, only a small number of molecules that bind to this cavity can inhibit YAP activity. This cavity and is flexible to accommodate molecules of diverse structure and it is

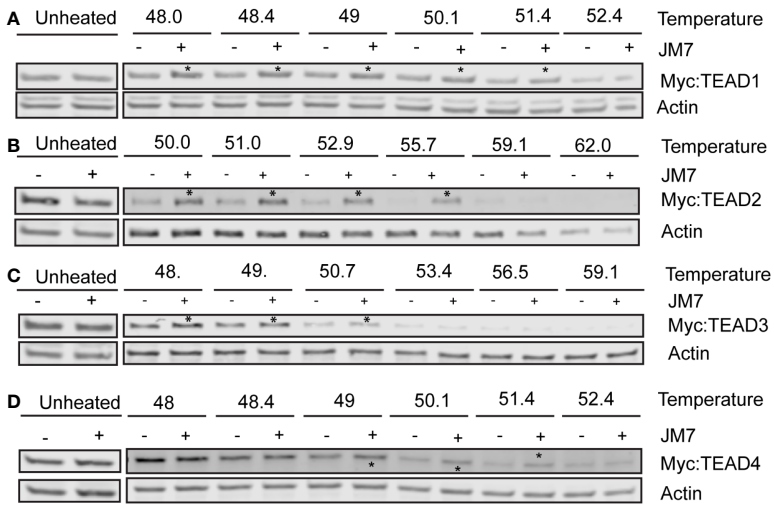

FIGURE 5
JM7 engages with TEAD1-4 in cells. **(A–D)** Representative Western blots showing amount of Myc-TEAD1-4 present in the supernatant following Cellular Thermal Shift Assay (CETSA). HEK293 cells expressing Myc-TEAD1-4 were treated with DMSO or 10 micromolar JM7 for 4 hours to avoid TEAD degradation, and CETSA was performed. Asterisks indicate stabilization of JM7-bound TEAD. All CETSA experiments were performed with at least 5 independent replicates.

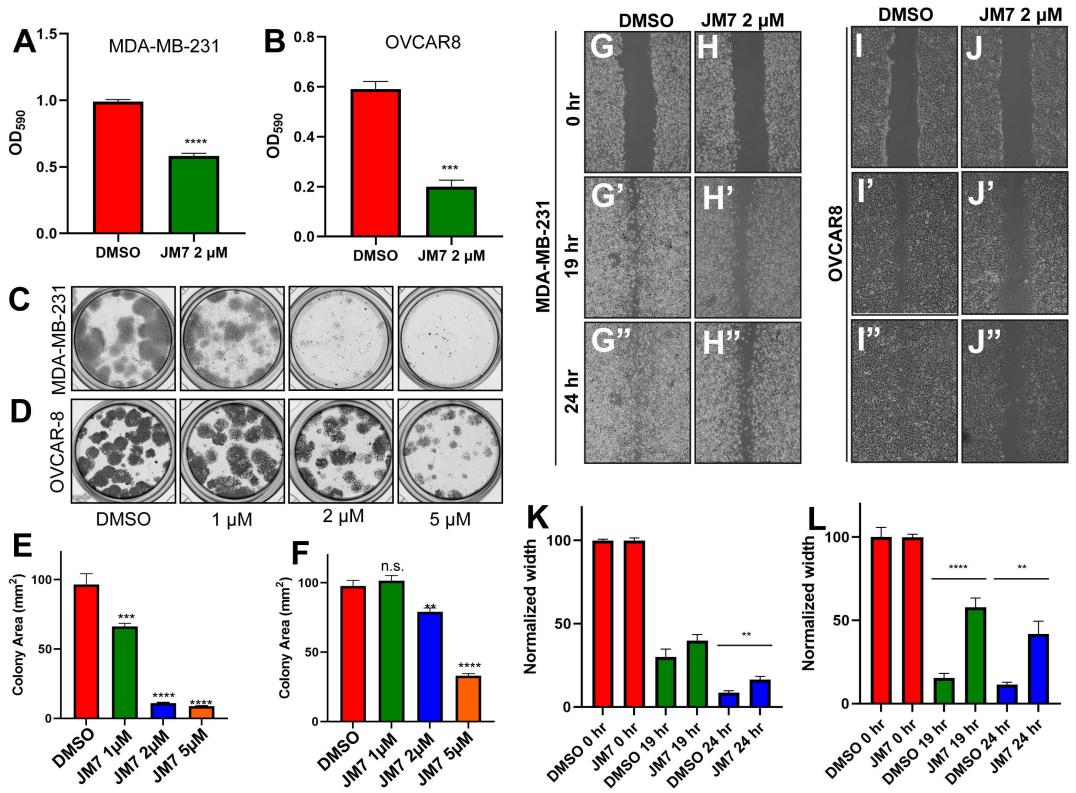

FIGURE 6
JM7 inhibits proliferation, colony formation and migration of breast and ovarian cancer cells. **(A, B)**. MTT assay for MDA-MB-231 cells **(A)** and OVCAR-8 cells **(B)** treated with DMSO or the indicated doses of JM7, showing inhibition of proliferation of these cancer cells by JM7. **(C–F)** Representative images showing colony formation assay for MDA-MB-231 **(C)** and OVCAR-8 cells **(D)** treated with DMSO or 1, 2 or 5 micromolar JM7. **(E, F)** Histograms showing normalized colony area for DMSO and JM7 treated MDA-MB-231 **(E)** and OVCAR-8 **(F)**. **(G–J")** Representative images showing wound healing assay for MDA-MB-231 **(G, H")** and OVCAR-8 cells **(I, J")** treated with DMSO or 2 micromolar JM7. **(K, L)** Histograms showing normalized wound width for DMSO and JM7 treated MDA-MB-231 **(K)** and OVCAR-8 **(L)** cells at 0, 19 and 24 hours. **(K, L)** **p <0.05; ***p <0.005; ****p <0.001. n.s: not significant. Error bars indicate Standard Error of Mean (SEM) of three replicates. Please also see Figure S2.

likely that only molecules that induce conformational change in TEAD to disrupt its interaction with YAP/TAZ and/or promote its degradation (42). The molecular features that endow this property to some inhibitors remain unknown, and identification of diverse chemical structures that inhibit YAP activity will enable develop computational models for better prediction of inhibitors.

It has been shown that TEAD palmitoylation is not required for its nuclear localization but required for TEAD stability and its interaction with YAP/TAZ (32). Consistent with this, we observed that JM7 inhibited palmitoylation of all four TEAD isoforms but did not affect TEAD or YAP localization. Further, consistent with previous reports, we observed that JM7 treatment destabilized all the 4 TEAD isoforms. Interestingly, we observed JM7 affects stability of the different TEAD isoforms differently. Especially, the destabilizing effect was not as drastic in case of TEAD3. This could be due to less efficient inhibition of palmitoylation or higher expression of TEAD3. The volume of the palmitic acid binding pocket in TEAD3 is significantly different than the other isoforms due to Y230, V331 and F414 (43). Further, Y230 and F414 are predicted to profoundly influence the shape of this site. Another possibility could be that the different TEAD isoforms have different stability in unpalmitoylated state. TEAD3 expression is limited to placental tissues. This could explain JM7 has a strong inhibitory effect on YAP target gene expression in three different cancer cell lines. Further structure activity studies will be required to further improve JM7 to develop analogs that can potently inhibit all the four TEAD isoforms.

Loss of NF2 function is commonly detected in many cancers including malignant mesothelioma, meningioma and schwannoma (10). MDA-MB-231 and NCI-226 cells also harbor mutations in NF2, which causes activation of YAP in these cells (44). JM7 inhibits YAP target gene expression,

viability, proliferation and migration of these cells. Further investigations will be required to examine if JM7 is effective in other cancers with NF2 mutation. Similarly, in many cancers YAP/TAZ are overexpressed by upstream oncogenic signaling pathways such as EGFR, RAS-MAPK, PI3, WNT, and exhibit increased YAP nuclear localization. Therefore, we posit that JM7 will be effective in many cancers that exhibit high expression and nuclear localization of YAP/TAZ. Further increased YAP nuclear localization has also been reported to be associated with chemotherapy resistance and relapse in EGFR-mutant, KRAS-mutant and B-RRAF mutant, ALK-rearranged non-small-cell lung cancer and RAS-driven neuroblastoma (19, 22, 45–51). TEAD palmitoylation inhibitors such as JM7 will be potentially useful adjunct therapy along with these pathway specific inhibitors. Similarly, increased YAP activity in cancer cells and immune cells interferes with immunotherapy (19, 22, 24–28). Therefore, JM7 will be potentially useful in combination with immunotherapy such as immune check point inhibitors.

YAP and TAZ also play a critical role in cancer associated fibroblasts and stimulate fibrosis, which in turn activates YAP, thereby creating a vicious feed forward loop. Similarly, they play a critical role in pulmonary, hepatic and renal fibrosis, where downstream of TGF-β signaling, YAP/TAZ plays a pivotal role in promoting conversion of the fibroblasts into myofibroblasts and induce expression of genes encoding ECM components (52). We propose that JM7 may be effective in fibrotic conditions, where YAP/TAZ plays a prominent role. Further investigations will be required for assessing the *in vivo* efficacy of JM7 in cancer and fibrosis. Moreover, new analogs can be synthesized and tested to develop more potent TEAD inhibitors with desirable pharmacological properties.

Experimental procedures

Molecular docking

The X-ray crystal structure of TEAD2 was retrieved from the protein Data Bank (PDB ID: 6UYC) and was prepared in the protein preparation wizard of Schrodinger. Missing side chains were added using Prime implemented in Maestro. Hydrogens were added and bond orders were assigned. The resulting structure was protonated at pH 7.0 using PROPKA. The ligands were retrieved from PubChem, prepared using LigPrep wizard in Maestro and protonated at pH 7.0 using Epik. Subsequently, energy minimization was performed using OPLS5 force field within 0.3A° root mean square deviation. Docking was performed using the Ligand docking workflow in Glide using Standard Precision mode (Glide SP). The top 25% of the compounds was subjected to Xtra precision (XP) docking and MM-GBSA. The compounds with the lowest dG-Bind score were chosen for testing how they affect YAP transcriptional reporter.

Molecular biology

pCMX-GAL4-TEAD1 (Addgene #33108), pCMX-GAL4-TEAD2 (Addgene #33107), pCMX-GAL4-TEAD3 (Addgene #33106), pCMX-GAL4-TEAD4 (Addgene #33105), pRK5-Myc-TEAD4 (Addgene #24638), GST-YAP2 (Addgene #24637), pCMV-FLAG-YAP-5SA/S94A (Addgene #33103), and pCDNA3-HA-TAZ (Addgene #32839) were obtained from Addgene. The human codon-optimized TEAD3 coding sequence with N-terminal Myc tag was synthesized as a gBlock (Integrated DNA Technologies). Full length TEAD1 and TEAD2 coding sequences were amplified from pCMX-GAL4-TEAD1 and pCMX-GAL4-TEAD2 and cloned into the EcoRI site of pCDNA3.1 by Gibson assembly using the NEBuilder® HiFi DNA Assembly Kit (New England Biolabs Cat. #E2621). The TEAD3 gBlock fragment was similarly cloned into the EcoRI site of pCDNA3.1 by Gibson assembly. pCDNA3.1-TAZ-S89A was generated by creating overlapping fragments to mutate the target residue and ligated by Gibson assembly into the EcoRI site of pCDNA3.1. SmBiT-YAP, SmBiT-TAZ and LgBiT-TEAD1 were synthesized as gBlock fragments and cloned into the EcoRI site of pCDNA3.1 by Gibson assembly. The LgBiT-TEAD1 subsequently used as template to amplify the LgBit fragment of Nanoluc; TEAD2-YBD was amplified from pCMX-GAL4-TEAD2, TEAD3-YBD from pDONR221-TEAD3, and TEAD4-YBD from pRK5-Myc-TEAD4. pCDNA3.1-LgBiT-TEAD2, pCDNA3.1-LgBiT-TEAD3 and pCDNA3.1-LgBiT-TEAD4 were then constructed by Gibson assembly of their respective fragments into the EcoRI site of pCDNA3.1. All the primers used for cloning in this study are listed in Supplementary Table 2.

Cell culture and transfections

HEK-293, MDA-MB-231, and NCI-H226 cells were obtained from ATCC and OVCAR-8 cells were obtained from National Cancer Institute and cultured in Dulbecco's Modified Eagle's Medium (DMEM, Corning Cat. #10-013-CV) supplemented with 10% heat-inactivated fetal bovine serum (HI FBS, Gibco™ Cat. #10438026) and 1% antibiotic/antimycotic (Gibco™). All cells were cultured in a humidified incubator at 37°C with 5% CO_2. HEK293 cells were transiently transfected using Lipofectamine 3000 (Invitrogen), following the manufacturer's protocol.

TEAD transcriptional reporter assay

8XGTIIC lentiviral particles were purchased from BPS Bioscience, Inc. and used to transduce HEK293 cells. Stable clones were established by selection with 2.5 μg/mL puromycin until distinct colonies formed. Colonies were established and stable clones were verified for YAP-dependent induction of luciferase expression by overexpressing YAP-5SA or TAZ-S89A. For dose

response assays, HEK293-8XGTIIC cells were transfected with either YAP-5SA or TAZ-S89A. One day after transfection, cells were seeded in triplicate in 96-well plates and treated with either vehicle control or JM7 (1, 2 and 5 μM) for 24 hr. A duplicate of each plate was seeded to allow for normalization to ATP levels by Cell Titer Glow. Luciferase assays were performed using a one-step luciferase assay kit (Promega), and ATP-based viability with Cell-Titer Glo 2.0 (Promega), following the manufacturer's protocol. Luminescence data was recorded on a Promega Glo-Max Navigator instrument.

RNA extraction and RT-qPCR

MDA-MB-231, OVCAR-8 and NCI-226 cells were seeded at ~50% confluence in 6 well dishes and allowed to attach overnight. Cells were then treated with DMSO or JM7 (2 μM and 5 μM) for 24 hr. Total RNA was extracted with TRIzol reagent (Invitrogen), following the manufacturer's protocol. 1 μg of total RNA was reverse transcribed to cDNA using the iScript™ gDNA Clear cDNA synthesis kit (Bio-RAD). qPCR was performed with Applied Biosystems Fast SYBR Green master mix on an Applied Biosystems QuantStudio 6 Flex system. Target genes were normalized to GAPDH mRNA levels and relative fold changes calculated as $2^{-\Delta\Delta Ct}$. All the primers used for qRT-PCR in this study are listed in Supplementary Table 2.

Immunoprecipitation

Following transfection with the required plasmids and/or treatments, cells were trypsinized and collected in centrifuge tubes. Pellets were washed once with PBS, then lysed on ice for 30 minutes with PBS containing 0.5% IGEPAL-CA630 (Sigma-Aldrich) and cOmplete™ EDTA-free protease inhibitor cocktail. Following sonication and centrifugation at 4°C for 20 min at maximum speed, supernatants were collected and added to tubes containing 20 μL Pierce Protein-A agarose bead slurry (Thermo Scientific) and pre-cleared for 1 hour at 4°C. The pre-cleared supernatants were then added to tubes containing 50 μL Pierce anti-c-Myc agarose, EZview Red anti-FLAG/HA/Myc or V5-agarose affinity resins and incubated for 2 hours at 4°C. Immunoprecipitated protein was washed four times with PBS containing 0.5% IGEPAL-CA630 before proceeding to downstream assays such as palmitoylation assays or Western blotting.

Western blotting

Samples were treated with Laemmli buffer, boiled at 98°C for 5 minutes, then centrifuged at maximum speed for 2 min following which, the samples were resolved by SDS-PAGE and transferred to nitrocellulose membranes using a Bio-RAD Trans-Blot Turbo semi-dry transfer system. After blocking with protein-free blocking buffer (Li-COR), blots were incubated at 4°C overnight with anti-Myc and anti-actin primary antibodies. Next day, the blots were washed 4 times with PBST (PBS+1% Tween 20) and incubated with IR Dye 680 or IR Dye 780 conjugated secondary antibodies, or IR Dye 680 conjugated streptavidin (for palmitoylated fractions) for 1 hour at room temperature. After washing 4 times with PBST, the blots were scanned on a Li-COR Odyssey CLx system. The various antibodies used in this study are listed in Supplementary Table 3.

TEAD palmitoylation assay

HEK-293 cells transfected with Myc-TEAD1, Myc-TEAD2, Myc-TEAD3, or Myc-TEAD4 expression plasmids were treated with DMSO or 2 μM JM7 in conjunction with 100 μM alkyne palmitate for 24 hr. Myc-tagged TEAD was immunoprecipitated and alkyne palmitic acid was conjugated to biotin azide by click chemistry, where the precipitated TEAD proteins were incubated with 100 μL of reaction buffer containing 0.1mM biotin-azide, 1mM tris (2-carboxyethyl)phosphine (TCEP), 0.2mM tris (3-hydro xypropyltriazolylmethyl) amine (THPTA) and 1 mM $CuSO_4$. The reaction was carried out at 20°C for 1 hr with shaking at 1200 rpm and terminated by washing three times with PBS containing 0.5% IGEPAL-CA630. Subsequently, the samples were subjected to Western Blotting using IR Dye 680 conjugated streptavidin to detect the biotinylated palmitic acid.

Immunofluorescence

MDA-MB-231, OVCAR-8 and NCI-226 cells were seeded in 4-well chamber slides and allowed to attach overnight. Cells were then treated with DMSO or JM7 (2 μM) for 24 hr. After treatment, the media was removed, cells were washed with PBS, then fixed for 20 min with 4% PFA, permeabilized for 10 min with 0.5% Triton X-100 in PBS, then blocked for 30 min with 1% donkey serum and 0.1% Triton X-100 in PBS, followed by staining with anti-YAP (D8H1X, Cell Signaling Technology #14074) and anti-pan-TEAD (D3F7L, Cell Signaling Technology #13295) at 4°C overnight, then with appropriate Alexa Fluor 647-conjugated secondary antibodies for 1 hour at RT and counterstained nuclei with Hoechst for 5 min at RT. Slides were then overlaid with coverslip with Vectashield mounting medium and sealed with nail polish. Images were captured on a Leica TCS SP8 confocal laser scanning microscope and processed in Volocity.

The various antibodies used in this study are listed in Supplementary Table 3.

MTT assay

MTT assay was performed using the MTT assay kit (Abcam) following manufacturer's protocol. Briefly, equal number of MDA-

MB-231, OVCAR-8 or NCI-226 cells were plated in triplicate and were treated with DMSO or 2uM JM7 for 48 hours, following which they were incubated with the MTT reagent for 1 hours. The formazan crystals that formed were dissolved in the solubilization buffer and the absorbance was measured at 590nm wavelength.

Colony formation assay

Equal number of MDA-MB-231,OVCAR-8 or NCI-H226 cells were plated in triplicate and were treated with DMSO or 2uM JM7 for two weeks, following which they were fixed with 4% PFA and stained with 0.5% crystal violet dissolved in methanol. The images were acquired using Gelcount (Oxford Optronix) mammalian-cell colony, spheroid and organoid counter, and the colony areas were quantified using FIJI.

Wound healing/scratch assay

MDA-MB-231, OVCAR-8 or NCI-H226 cells were grown at full confluence and a scratch was made using a pipette tip. The detached cells were gently washed off with PBS and cells were incubated with media containing either DMSO or 2uM JM7. Images of the scratch areas were taken at 0, 19 and 24 hours following drug treatment and analyzed using FIJI.

NanoBiT complementation assay

HEK-293 cells were seeded at a density of 2×10^5 cells/mL in a 24 well dish and transfected with 250 ng of SmBiT-YAP, SmBiT-TAZ, LgBiT-TEAD1/2/3/4 alone or in combination. One day after transfection, cells were seeded in triplicate in 96-well plates and treated with either DMSO or JM7 (2 μM) for 24 hr. Nanoluc assays were performed using the Nano-Glo Luciferase assay kit, following the manufacturer's protocol. Luminescence was measured in a Promega Glo-Max Navigator instrument.

Statistical analysis

Results were recorded and sorted in Microsoft Excel and all statistical analyses were carried out using GraphPad Prism (San Diego, CA). Histograms show the mean plus Standard Error of Mean (SEM). All analyses were done with at least three independent replicates, unless otherwise stated. For pairwise comparisons we used two-tailed Student's t test for parametric distributions and a Mann-Whitney test for non-parametric distributions. For comparison of ratios, they were log transformed. For multiple comparisons, ANOVA was performed, and Tukey's *post hoc* test was performed and adjusted-p values were used for statistical inference.

Data availability statement

The original contributions presented in the study are included in the article/Supplementary Material Further inquiries can be directed to the corresponding author.

Author contributions

Conceptualization, JRM; methodology, AG, JRM; validation, AG, JRM; formal analysis, AG, JRM; investigation, AG, JRM; resources, JRM; data curation, JRM; writing-original draft preparation, AG, JRM; writing-review and editing, JRM; visualization, AG, JRM supervision, JRM; project administration, JRM; funding acquisition, JRM. SM is listed as an author since he refused to sign the author removal form. All authors have read and agreed to the published version of the manuscript.

Funding

This research was funded by University of Texas at Dallas Start-up funds and SPIRe Grant to JRM.

Acknowledgments

We thank the Misra lab members for their critical inputs on the manuscript. We thank Nikki Delk for the kind gift of MDA-MB-231 cells and Dr. Girgis Obaid for kindly allowing us to use the Gelcount colony imager.

Conflict of interest

The authors declare that the research was conducted in the absence of any commercial or financial relationships that could be construed as a potential conflict of interest.

Publisher's note

Supplementary material

The Supplementary Material for this article can be found online at: https://www.frontiersin.org/articles/10.3389/fonc.2022.1021823/full#supplementary-material

References

1. Misra JR, Irvine KD. The hippo signaling network and its biological functions. *Annu Rev Genet* (2018) 52:65–87. doi: 10.1146/annurev-genet-120417-031621

2. Ma S, Meng Z, Chen R, Guan KL. The hippo pathway: Biology and pathophysiology. *Annu Rev Biochem* (2019) 88:577–604. doi: 10.1146/annurev-biochem-013118-111829

3. Meng Z, Moroishi T, Mottier-Pavie V, Plouffe SW, Hansen CG, Hong AW, et al. MAP4K family kinases act in parallel to MST1/2 to activate LATS1/2 in the hippo pathway. *Nat Commun* (2015) 6:8357. doi: 10.1038/ncomms9357

4. Plouffe SW, Meng Z, Lin KC, Lin B, Hong AW, Chun JV, et al. Characterization of hippo pathway components by gene inactivation. *Mol Cell* (2016) 64:993–1008. doi: 10.1016/j.molcel.2016.10.034

5. Battilana G, Zanconato F, Piccolo S. Mechanisms of YAP/TAZ transcriptional control. *Cell Stress* (2021) 5:167–72. doi: 10.15698/cst2021.11.258

6. Lopez-Hernandez A, Sberna S, Campaner S. Emerging principles in the transcriptional control by YAP and TAZ. *Cancers (Basel)* (2021) 13(16):4242. doi: 10.3390/cancers13164242

7. Zanconato F, Cordenonsi M, Piccolo S. YAP and TAZ: a signalling hub of the tumour microenvironment. *Nat Rev Cancer* (2019) 19:454–64. doi: 10.1038/s41568-019-0168-y

8. Dey A, Varelas X, Guan KL. Targeting the hippo pathway in cancer, fibrosis, wound healing and regenerative medicine. *Nat Rev Drug Discov* (2020) 19:480–94. doi: 10.1038/s41573-020-0070-z

9. Yin F, Yu J, Zheng Y, Chen Q, Zhang N, Pan D. Spatial organization of hippo signaling at the plasma membrane mediated by the tumor suppressor Merlin/NF2. *Cell* (2013) 154:1342–55. doi: 10.1016/j.cell.2013.08.025

10. Petrilli AM, Fernandez-Valle C. Role of Merlin/NF2 inactivation in tumor biology. *Oncogene* (2016) 35:537–48. doi: 10.1038/onc.2015.125

11. Hmeljak J, Sanchez-Vega F, Hoadley KA, Shih J, Stewart C, Heiman D, et al. Integrative molecular characterization of malignant pleural mesothelioma. *Cancer Discovery* (2018) 8:1548–65. doi: 10.1158/2159-8290.CD-18-0804

12. Bueno R, Stawiski EW, Goldstein LD, Durinck S, De Rienzo A, Modrusan Z, et al. Comprehensive genomic analysis of malignant pleural mesothelioma identifies recurrent mutations, gene fusions and splicing alterations. *Nat Genet* (2016) 48:407–16. doi: 10.1038/ng.3520

13. Lee S, Karas PJ, Hadley CC, Bayley VJ, Khan AB, Jalali A, et al. The role of Merlin/NF2 loss in meningioma biology. *Cancers (Basel)* (2019) 11(11):1633. doi: 10.3390/cancers11111633

14. Lo Sardo F, Strano S, Blandino G. YAP and TAZ in lung cancer: Oncogenic role and clinical targeting. *Cancers (Basel)* (2018) 10(5):137. doi: 10.3390/cancers10050137

15. Merritt N, Garcia K, Rajendran D, Lin ZY, Zhang X, Mitchell KA, et al. TAZ-CAMTA1 and YAP-TFE3 alter the TAZ/YAP transcriptome by recruiting the ATAC histone acetyltransferase complex. *eLife* (2021) 10:e62857. doi: 10.7554/eLife.62857.sa2

16. Driskill JH, Zheng Y, Wu BK, Wang L, Cai J, Rakheja D, et al. WWTR1 (TAZ)-CAMTA1 reprograms endothelial cells to drive epithelioid hemangioendothelioma. *Genes Dev* (2021) 35:495–511. doi: 10.1101/gad.348221.120

17. Seavey CN, Pobbati AV, Hallett A, Ma S, Reynolds JP, Kanai R, et al. WWTR1(TAZ)-CAMTA1 gene fusion is sufficient to dysregulate YAP/TAZ signaling and drive epithelioid hemangioendothelioma tumorigenesis. *Genes Dev* (2021) 35:512–27. doi: 10.1101/gad.348220.120

18. Tanas MR, Ma S, Jadaan FO, Ng CK, Weigelt B, Reis-Filho JS, et al. Mechanism of action of a WWTR1(TAZ)-CAMTA1 fusion oncoprotein. *Oncogene* (2016) 35:929–38. doi: 10.1038/onc.2015.148

19. Yu M, Peng Z, Qin M, Liu Y, Wang J, Zhang C, et al. Interferon-gamma induces tumor resistance to anti-PD-1 immunotherapy by promoting YAP phase separation. *Mol Cell* (2021) 81:1216–230.e1219. doi: 10.1016/j.molcel.2021.01.010

20. Lu Y, Wu T, Gutman O, Lu H, Zhou Q, Henis YI, et al. Phase separation of TAZ compartmentalizes the transcription machinery to promote gene expression. *Nat Cell Biol* (2020) 22:453–64. doi: 10.1038/s41556-020-0485-0

21. Cai D, Feliciano D, Dong P, Flores E, Gruebele M, Porat-Shliom N, et al. Phase separation of YAP reorganizes genome topology for long-term YAP target gene expression. *Nat Cell Biol* (2019) 21:1578–89. doi: 10.1038/s41556-019-0433-z

22. Nguyen CDK, Yi C. YAP/TAZ signaling and resistance to cancer therapy. *Trends Cancer* (2019) 5:283–96. doi: 10.1016/j.trecan.2019.02.010

23. Park JH, Shin JE, Park HW. The role of hippo pathway in cancer stem cell biology. *Mol Cells* (2018) 41:83–92. doi: 10.14348/molcells.2018.2242

24. Wang G, Lu X, Dey P, Deng P, Wu CC, Jiang S, et al. Targeting YAP-dependent MDSC infiltration impairs tumor progression. *Cancer Discov* (2016) 6:80–95. doi: 10.1158/2159-8290.CD-15-0224

25. Ni X, Tao J, Barbi J, Chen Q, Park BV, Li Z, et al. YAP is essential for treg-mediated suppression of antitumor immunity. *Cancer Discov* (2018) 8:1026–43. doi: 10.1158/2159-8290.CD-17-1124

26. Kim MH, Kim CG, Kim SK, Shin SJ, Choe EA, Park SH, et al. YAP-induced PD-L1 expression drives immune evasion in BRAFi-resistant melanoma. *Cancer Immunol Res* (2018) 6:255–66. doi: 10.1158/2326-6066.CIR-17-0320

27. Miao J, Hsu PC, Yang YL, Xu Z, Dai Y, Wang Y, et al. YAP regulates PD-L1 expression in human NSCLC cells. *Oncotarget* (2017) 8:114576–87. doi: 10.18632/oncotarget.23051

28. Lee BS, Park DI, Lee DH, Lee JE, Yeo MK, Park YH, et al. Hippo effector YAP directly regulates the expression of PD-L1 transcripts in EGFR-TKI-resistant lung adenocarcinoma. *Biochem Biophys Res Commun* (2017) 491:493–9. doi: 10.1016/j.bbrc.2017.07.007

29. Barry ER, Simov V, Valtingojer I, Venier O. Recent therapeutic approaches to modulate the hippo pathway in oncology and regenerative medicine. *Cells* (2021) 10(10):2715. doi: 10.3390/cells10102715

30. Pobbati AV, Rubin BP. Protein-protein interaction disruptors of the YAP/TAZ-TEAD transcriptional complex. *Molecules* (2020) 25(24):6001. doi: 10.3390/molecules25246001

31. Smith SA, Sessions RB, Shoemark DK, Williams C, Ebrahimighaei R, McNeill MC, et al. Antiproliferative and antimigratory effects of a novel YAP-TEAD interaction inhibitor identified using in silico molecular docking. *J Med Chem* (2019) 62:1291–305. doi: 10.1021/acs.jmedchem.8b01402

32. Chan P, Han X, Zheng B, DeRan M, Yu J, Jarugumilli GK, et al. Autopalmitoylation of TEAD proteins regulates transcriptional output of the hippo pathway. *Nat Chem Biol* (2016) 12:282–9. doi: 10.1038/nchembio.2036

33. Noland CL, Gierke S, Schnier PD, Murray J, Sandoval WN, Sagolla M, et al. Palmitoylation of TEAD transcription factors is required for their stability and function in hippo pathway signaling. *Structure* (2016) 24:179–86. doi: 10.1016/j.str.2015.11.005

34. Tang TT, Konradi AW, Feng Y, Peng X, Ma M, Li J, et al. Small molecule inhibitors of TEAD auto-palmitoylation selectively inhibit proliferation and tumor growth of NF2-deficient mesothelioma. *Mol Cancer Ther* (2021) 20:986–98. doi: 10.1158/1535-7163.MCT-20-0717

35. Holden JK, Crawford JJ, Noland CL, Schmidt S, Zbieg JR, Lacap JA, et al. Small molecule dysregulation of TEAD lipidation induces a dominant-negative inhibition of hippo pathway signaling. *Cell Rep* (2020) 31:107809. doi: 10.1016/j.celrep.2020.107809

36. Bum-Erdene K, Zhou D, Gonzalez-Gutierrez G, Ghozayel MK, Si Y, Xu D, et al. Small-molecule covalent modification of conserved cysteine leads to allosteric inhibition of the TEADYap protein-protein interaction. *Cell Chem Biol* (2019) 26:378–89.e313. doi: 10.1016/j.chembiol.2018.11.010

37. Gorgulla C, Boeszoermenyi A, Wang ZF, Fischer PD, Coote PW, Padmanabha Das KM, et al. An open-source drug discovery platform enables ultra-large virtual screens. *Nature* (2020) 580:663–8. doi: 10.1038/s41586-020-2117-z

38. Sadybekov AA, Sadybekov AV, Liu Y, Iliopoulos-Tsoutsouvas C, Huang XP, Pickett J, et al. Synthon-based ligand discovery in virtual libraries of over 11 billion compounds. *Nature* (2021) 601:452–59. doi: 10.1038/s41586-021-04220-9

39. Bender BJ, Gahbauer S, Luttens A, Lyu J, Webb CM, Stein RM, et al. A practical guide to large-scale docking. *Nat Protoc* (2021) 16:4799–832. doi: 10.1038/s41596-021-00597-z

40. Nouri K, Azad T, Ling M, Janse van Rensburg HJ, Pipchuk A, Shen H, et al. Identification of celastrol as a novel YAP-TEAD inhibitor for cancer therapy by high throughput screening with ultrasensitive YAP/TAZ-TEAD biosensors. *Cancers (Basel)* (2019) 11(10):1596. doi: 10.3390/cancers11101596

41. Jafari R, Almqvist H, Axelsson H, Ignatushchenko M, Lundback T, Nordlund P, et al. The cellular thermal shift assay for evaluating drug target interactions in cells. *Nat Protoc* (2014) 9:2100–22. doi: 10.1038/nprot.2014.138

42. Liberelle M, Toulotte F, Renault N, Gelin M, Allemand F, Melnyk P, et al. Toward the design of ligands selective for the c-terminal domain of TEADs. *J Med Chem* (2022) 65:5926–40. doi: 10.1021/acs.jmedchem.2c00075

43. Heinrich T, Peterson C, Schneider R, Garg S, Schwarz D, Gunera J, et al. Optimization of TEAD p-site binding fragment hit into *In vivo* active lead MSC-4106. *J Med Chem* (2022) 65:9206–29. doi: 10.1021/acs.jmedchem.2c00403

44. Dupont S, Morsut L, Aragona M, Enzo E, Giulitti S, Cordenonsi M, et al. Role of YAP/TAZ in mechanotransduction. *Nature* (2011) 474:179–83. doi: 10.1038/nature10137

45. Mudianto T, Campbell KM, Webb J, Zolkind P, Skidmore ZL, Riley R, et al. Yap1 mediates trametinib resistance in head and neck squamous cell carcinomas. *Clin Cancer Res* (2021) 27:2326–39. doi: 10.1158/1078-0432.CCR-19-4179

46. Gonzalez-Alonso P, Zazo S, Martin-Aparicio E, Luque M, Chamizo C, Sanz-Alvarez M, et al. The hippo pathway transducers YAP1/TEAD induce acquired resistance to trastuzumab in HER2-positive breast cancer. *Cancers (Basel)* (2020) 12(5):1108. doi: 10.3390/cancers12051108

47. Song Y, Sun Y, Lei Y, Yang K, Tang R. YAP1 promotes multidrug resistance of small cell lung cancer by CD74-related signaling pathways. *Cancer Med* (2020) 9:259–68. doi: 10.1002/cam4.2668

48. Nilsson MB, Sun H, Robichaux J, Pfeifer M, McDermott U, Travers J, et al. A YAP/FOXM1 axis mediates EMT-associated EGFR inhibitor resistance and increased expression of spindle assembly checkpoint components. *Sci Trans Med* (2020) 12(559):eaaz4589. doi: 10.1126/scitranslmed.aaz4589

49. Coggins GE, Farrel A, Rathi KS, Hayes CM, Scolaro L, Rokita JL, et al. YAP1 mediates resistance to MEK1/2 inhibition in neuroblastomas with hyperactivated RAS signaling. *Cancer Res* (2019) 79:6204–14. doi: 10.1158/0008-5472.CAN-19-1415

50. Lin L, Sabnis AJ, Chan E, Olivas V, Cade L, Pazarentzos E, et al. The hippo effector YAP promotes resistance to RAF- and MEK-targeted cancer therapies. *Nat Genet* (2015) 47:250–6. doi: 10.1038/ng.3218

51. Tsuji T, Ozasa H, Aoki W, Aburaya S, Yamamoto Funazo T, Furugaki K, et al. YAP1 mediates survival of ALK-rearranged lung cancer cells treated with alectinib *via* pro-apoptotic protein regulation. *Nat Commun* (2020) 11:74. doi: 10.1038/s41467-019-13771-5

52. Tschumperlin DJ, Ligresti G, Hilscher MB, Shah VH. Mechanosensing and fibrosis. *J Clin Invest* (2018) 128:74–84. doi: 10.1172/JCI93561